BULLETIN OF THE POLISH ACADEMY OF SCIENCES
TECHNICAL SCIENCES, Vol. 61, No. 1, 2013
*DOI: 10.2478/bpasts-2013-0009*



# Smoothed particle hydrodynamics versus finite element method for blast impact

T. JANKOWIAK* and T. ŁODYGOWSKI

Institute of Structural Engineering, Poznan University of Technology, 5 Piotrowo St., 61-138 Poznan, Poland

**Abstract.** The paper considers the failure study of concrete structures loaded by the pressure wave due to detonation of an explosive material. In the paper two numerical methods are used and their efficiency and accuracy are compared. There are the Smoothed Particle Hydrodynamics (SPH) and the Finite Element Method (FEM). The numerical examples take into account the dynamic behaviour of concrete slab or a structure composed of two concrete slabs subjected to the blast impact coming from one side. The influence of reinforcement in the slab (1, 2 or 3 layers) is also presented and compared with a pure concrete one. The influence of mesh density for FEM and the influence of important parameters in SPH like a smoothing length or a particle distance on the quality of the results are discussed in the paper.

**Key words:** FEM, SPH, blast impact, concrete slab.

## 1. Introduction

In the recent years the description of the critical infrastructure security has become a very important topic [1, 2]. Generally, the problem is connected with the acts of terrorism. First cases appear more than 2000 years ago [3] so it means that it is not a new phenomenon. To protects the buildings and to increase their security of the new designed ones and those which exist, they are redesigned and reinforced by some additional elements [4]. The goal is to adapt these buildings to the new requirements and improve their safety. The crucial is to assure the safety of the structures under exceptional loads, such as the pressure wave caused by explosion[5,6] or missile impact [7].

The rules which significantly improve the safety are usually created based on the essential conditions derived directly from experiments and previous experiences and observations. To reduce the expensive experiments in foreseeing the final effects the numerical simulations could be successfully used. The numerical models are accepted only if all parts of the structure as well as the description of processes are modelled accurately. The simulations of the experiments with explosives and missile impacts are crucial for better understanding what could happen in buildings or its parts in critical situations. Computer simulations can successfully help to determine the damage or even destruction of the whole building or its structural part [8].

This work focuses on determination of the damage and structural failure using two numerical methods the Finite Element (FE) and the Smoothed Particle Hydrodynamic (SPH) and on comparison of the quality of obtained results. The analyses of the pure single and double slabs and also reinforced concrete slabs subjected to impact pressure loadings generated by the explosion serve for the comparison of the two mentioned numerical methods.

*e-mail: tomasz.jankowiak@put.poznan.pl

## 2. The object under analyses

The structure under consideration is a concrete slab or the set of two parallel concrete slabs with a gap between them. The dimensions of the square slab, which is presented in Fig. 1, are 1 m by 1 m with the thickness of 0.2 m. The slabs are fixed on perimeter and the distance between slabs in the second case is 0.1 m. The considered structure is loaded by the wave pressure caused by explosion of TNT and the mass of charge varies between 25 kg and 600 kg. The charge is placed in a distance of 1.8 m from the slab's surface, see Fig. 1. The details on the wave intensity and modelling the pressure distribution that acts on an obstacle (slab) could be found in literature [9].

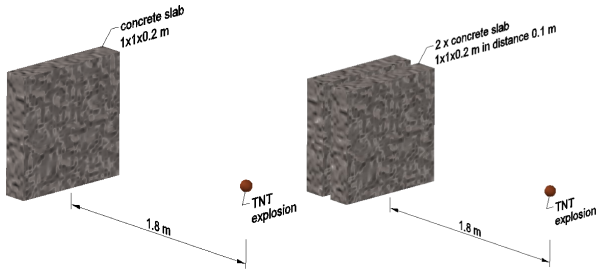


Fig. 1. The geometry of the concrete slabs

The slabs are made of a concrete B30. The quasi-static uniaxial compressive strength is equal to 30 MPa. The quasi-static and dynamic mechanical behaviour of the considered concrete is presented in Fig. 2. The stress-strain curve for uniaxial compression and tension is presented in Fig. 2-A. The failure curve in the space of plane stresses is presented in Fig. 2-B. The compressive and tensile dynamic increase factors versus strain rates are shown in Figs. 2-C and 2-D, respectively. It is well known from experiments that increase factors are growing substantially with the rate of deformations reaching the values over 2 for compression and of order 10 for tension.

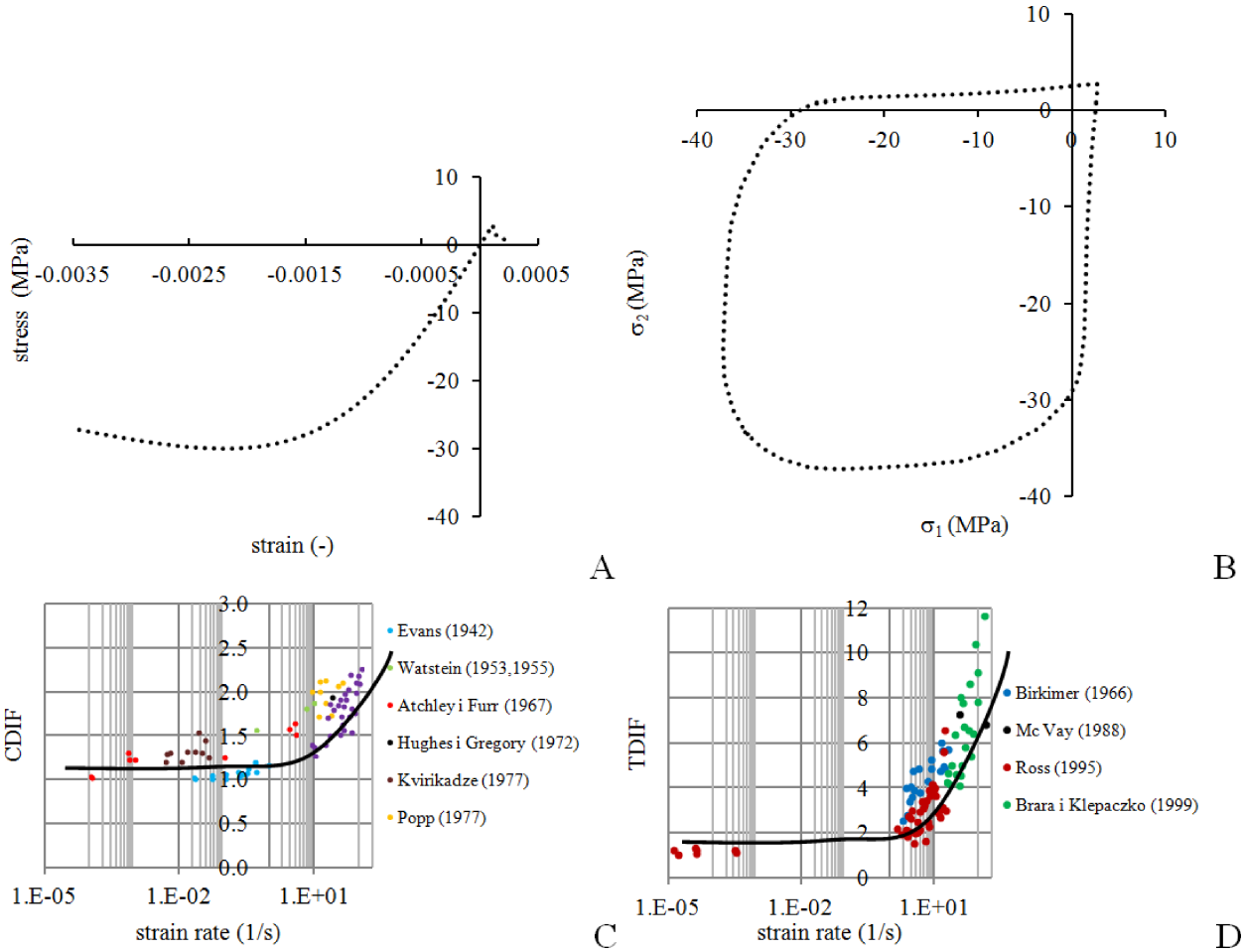


Fig. 2. Quasi-static and dynamic behaviours of concrete B30; A – uniaxial compression and tension, B – failure curve in plane state of stress, C – Compressive Dynamic Increase Factor CDIF versus strain rate, D – Tensile Dynamic Increase Factor TDIF versus strain rate

## 3. Numerical model

The two numerical methods are used to analyse the problem of dynamic behaviour of concrete slabs subjected to the explosion pressure wave. First the Finite Element Method – FEM [10] is considered and second the Smoothed Particle Hydrodynamics – SPH [10–12] is employed. There are different possibilities to model the distribution of pressure wave on the structure. It can be done by the analysis of travelling waves in the space which ends with the estimation of pressure on the obstacle [9]. In our consideration to avoid the complex analysis of the moving waves in the air the ConWep loading function is used to simulate the explosive pressure wave [13]. The analyses contain the influence of the mesh size (FEM) and particle distance (SPH). The accurate description of the influence of SPH method parameters like particle distance, smoothing length etc is presented in detail in Appendix A.

Complex material model to simulate dynamic behaviour of concrete is important to describe properly different effects [12, 14]. In the work we have used the model which consists of the material of the elastic-plastic behaviour with initiation of damage in accumulative form [15]. The evolution of damage and failure is mode dependent and regularisation has to be introduced here also in energetic form. The strain rate effects are also introduced into the model. The more detailed description is presented below.

The continuous damage surface cap model is used to simulate the concrete behaviour and properties [14, 16]. The parameters presented below are considered in material simulations. The elastic state is fully described by only two parameters $G$ and $K$. The first is the shear modulus and the second one is the bulk modulus, respectively. The material density $\rho$ needs to be also defined in dynamic analysis while the inertia forces play an important role. In the model the associated flow rule is used. The yield criterion is used in the following form:

$$f\left(J_1, J_2', J_3', \kappa\right) = J_2' - \Re^2 F_f^2 F_c, \tag{1}$$

where $J_1$ is the first invariant of stress tensor, $J_2'$ is the second invariant of stress deviator, $J_3'$ is the third invariant of stress deviator and $\kappa$ is the cap hardening parameter. The shear failure surface $F_f$ is expressed in the following form:

$$F_f = \alpha - \lambda e^{-\beta J_1} + \theta J_1. \tag{2}$$

The material parameters $\alpha$, $\beta$, $\lambda$ and $\theta$ describe the shear failure surface, see Table 1. In Eq. (1) the Rubin scaling func-

tion $\Re$ is used to reduce the concrete strength in torsion and under triaxial tension. This function is of the following form:

$$\Re = \begin{bmatrix} Q_1 = \alpha_1 - \lambda_1 e^{-\beta_1 J_1} + \theta_1 J_1 & \text{torsion} \\ Q_2 = \alpha_2 - \lambda_2 e^{-\beta_2 J_1} + \theta_2 J_1 & \text{triaxial extension} \end{bmatrix}. \quad (3)$$

Table 1
Parameters for concrete B30

| | |
|---|---|
| $G = 11460$ MPa | $K = 12550$ MPa |
| $\rho = 2320 \cdot 10^{-12}$ t/mm$^2$ | $\alpha = 14.5$ MPa |
| $\alpha_1 = 0.7473$ | $\alpha_2 = 0.66$ |
| $\lambda = 10.5$ MPa | $\lambda_1 = 0.17$ |
| $\lambda_2 = 0.16$ | $\beta = 0.01929$ MPa$^{-1}$ |
| $\beta_1 = 0.07057$ MPa$^{-1}$ | $\beta_2 = 0.07057$ MPa$^{-1}$ |
| $\theta = 0.2965$ | $\theta_1 = 1.151 \cdot 10^{-3}$ MPa$^{-1}$ |
| $\theta_2 = 1.387 \cdot 10^{-3}$ MPa$^{-1}$ | $R = 5$ |
| $B = 100$ | $pwrc = 5$ |
| $X_0 = 90.54$ MPa | $G_{fc} = 6.838$ MPa·mm |
| $N_t = 0.48$ | $W = 0.05$ |
| $D = 0.1$ | $N_c = 0.78$ |
| $D_1 = 2.5 \cdot 10^{-4}$ MPa | $G_{ft} = 0.06838$ MPa·mm |
| $\eta_{0t} = 6.176 \cdot 10^{-5}$ s | $D_2 = 3.49 \cdot 10^{-7}$ MPa$^2$ |
| $G_{fs} = 0.06838$ MPa·mm | $\eta_{0c} = 1.003 \cdot 10^{-4}$ s |
| $pmod = 0$ | $pwrt = 1$ |
| $S_{rate} = 1$ | $\tau_{0c} = 0.1322$ MPa$^{0.5}$ |
| $\tau_{0t} = 0.0152$ MPa$^{0.5}$ | $repow = 1$ |
| $\kappa_0 = 45$ MPa | |

The material parameters $\alpha_1$, $\alpha_2$, $\beta_1$, $\beta_2$, $\lambda_1$, $\lambda_2$, $\theta_1$ and $\theta_2$ describe the Rubin scaling function, see Table 1. The plastic potential function $f(J_1, J_2', J_3', \kappa)$ is limited by a cap hardening function in the case of triaxial compression. The function $F_c$ is presented as follows:

$$F_c(J_1, \kappa) = 1 - \frac{[J_1 - L(\kappa)]\,[|J_1 - L(\kappa)| + J_1 - L(\kappa)]}{2\,[X(\kappa) - L(\kappa)]^2}. \quad (4)$$

In Eq. (4) two other functions appear $L(\kappa)$ and $X(\kappa)$, where:

$$L(\kappa) = \begin{bmatrix} \kappa & \text{if} \quad \kappa > \kappa_0 \\ \kappa_0 & \text{if} \quad \kappa \le \kappa_0 \end{bmatrix} \quad (5)$$
$$\text{and } X(\kappa) = L(\kappa) + RF_f(L(\kappa)).$$

These functions describe the cap hardening limits. The two parameters $R$ and $\kappa_0$ describe the shape of the cap hardening function and $R$ is a cap aspect ratio but $\kappa_0$ is initial cap hardening. The plot of the plasticity surface including shear failure surface and cap hardening function is presented in Fig. 3. The cap hardening function serves as the limit condition for triaxial compression.

The cap moves during plastic deformation (volume change) according to the rule:

$$\varepsilon_v^{pl} = W\left(1 - e^{-D_1(X - X_0) - D_2(X - X_0)^2}\right). \quad (6)$$

The variable $\varepsilon_v^{pl}$ is a plastic volumetric strain and the parameters $W$, $D_1$, $D_2$, $X_0$ describe the expansion and contraction of the cap based on Eq. (6). In the model the scalar damage variable $d$ is used to describe the stress tensor with damage $\sigma_{ij}^d$ based on the visco-plastic stress tensor without damage $\sigma_{ij}^{vp}$, as follows:

$$\sigma_{ij}^d = (1 - d)\,\sigma_{ij}^{vp}, \quad (7)$$

with two independent damage mechanisms in compression (shear) and in tension. The two criteria of energetic type are used to describe the damage initiation and evolution. They are as follows:

$$\tau_c = \sqrt{\frac{1}{2}\sigma_{ij}\varepsilon_{ij}} \quad \text{if} \quad \begin{cases} J_1 & \text{compression} \\ \tau_c \ge \tau_{0c} & \text{energy} \end{cases}$$
$$\tau_t = \sqrt{E\varepsilon_{\max}^2} \quad \text{if} \quad \begin{cases} J_1 & \text{tension} \\ \tau_t \ge \tau_{0t} & \text{energy} \end{cases} \quad (8)$$

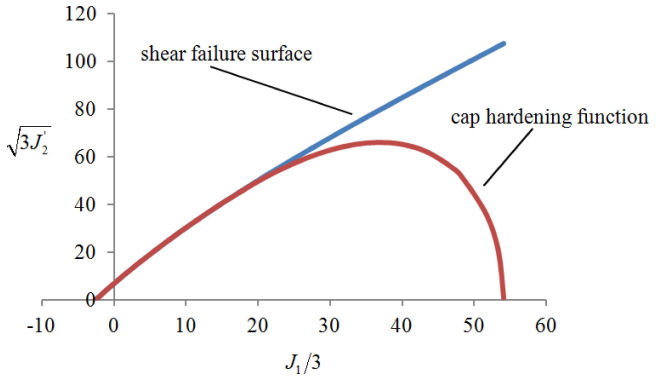


Fig. 3. Plasticity surface in meridian plane

The material parameters $\tau_{0c}$ and $\tau_{0c}$ describe the initiation values in compression and in tension, see Table 1. The two softening functions are used independently in shear and in tension in the following forms:

$$d(\tau_c) = \frac{d_{\max}}{B}\left[\frac{1 + B}{1 + Be^{-A(\tau_c - \tau_{0c})}} - 1\right] \text{ ductile damage,}$$
$$d(\tau_t) = \frac{0.999}{D}\left[\frac{1 + D}{1 + De^{-C(\tau_t - \tau_{0t})}} - 1\right] \text{ brittle damage.} \quad (9)$$

The variables $A$ and $C$ are equal characteristic finite element length $l_{el}$. Additionally, the variable $A$ may be reduced according to the following equation:

$$A = A(d_{max} + 0.001)^{pmod}. \quad (10)$$

The parameters $B$, $D$, $d_{\max}$, $pmod$ describe the shape of the softening functions in compression and in tension. The above softening functions, Eq. (9) are presented in Fig. 4 for two damage mechanisms and different element sizes (particle distance in SPH).

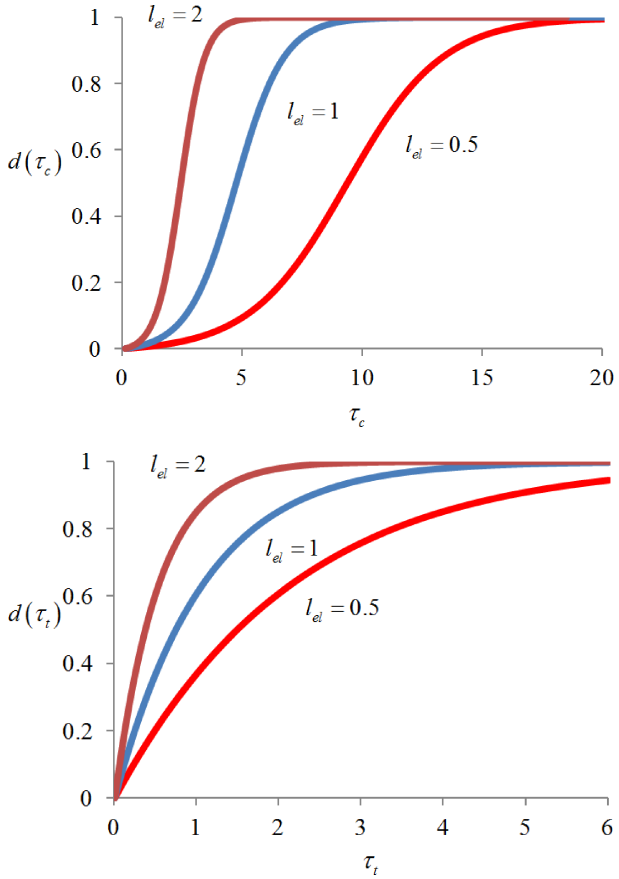


Fig. 4. The softening functions in compression (top) and in tension (bottom)

In the presented model the energy type regularization is used to obtain the unique solution independently of mesh size. The fracture damage energy $G_f$ depends on damage mechanism (state of stress) according to the following rules:

$$G_f = G_{fs} + \left(\frac{J_1}{\sqrt{3J_2'}}\right)^{pwrc} (G_{fc} - G_{fs})$$
for compressive pressure,
$$G_f = G_{fs} + \left(\frac{-J_1}{\sqrt{3J_2'}}\right)^{pwrt} (G_{ft} - G_{fs})$$
for tensile pressure. (11)

The parameters $G_{fs}$, $G_{ft}$, $G_{fc}$ describe the fracture energy in pure shear, in pure compression and in pure tension and $pwrt$, $pwrc$ are shear to tension and shear to compression transition parameters. The visco-plasticity formulation is used to consider the change in the material behaviour due to strain rates:

$$\sigma_{ij}^{vp} = (1-\gamma)\,\sigma_{ij}^{T} + \gamma\sigma_{ij}^{p} \quad \text{with} \quad \gamma = \frac{\Delta t/\eta}{1+\Delta t/\eta}. \tag{12}$$

The visco-plastic stress tensor without damage $\sigma_{ij}^{vp}$ is calculated based on elastic trial stress $\sigma_{ij}^{T}$ and inviscid stress tensor (without rate effect) $\sigma_{ij}^{p}$. The variable $\eta$ (an effective fluidity coefficient) in Eq. (12) is calculated independently for shear and for tension according to the following rules:

$$\eta = \eta_s + \left(\frac{J_1}{\sqrt{3J_2'}}\right)^{pwrc} (\eta_c - \eta_s)$$
for compressive pressure,
$$\eta = \eta_s + \left(\frac{-J_1}{\sqrt{3J_2'}}\right)^{pwrt} (\eta_t - \eta_s)$$
for tensile pressure. (13)

To calculate the variables $\eta_s$, $\eta_t$, $\eta_c$ the following equations are used:

$$\eta_t = \frac{\eta_{0t}}{\dot{\varepsilon}^{N_t}}, \qquad \eta_c = \frac{\eta_{0c}}{\dot{\varepsilon}^{N_c}}$$
and $\eta_s = S_{rate}\eta_t$. (14)

The material parameters $\eta_{0t}$, $\eta_{0c}$, $N_t$, $N_c$, $S_{rate}$ describe the fitting for uniaxial tension, compression and shear data. The variable $\dot{\varepsilon}$ describes the effective strain rate. The fracture damage energy depends on the strain rates according to the formula:

$$G_f^{rate} = G_f\left(1 + \frac{E\dot{\varepsilon}\eta}{f'}.\right)^{repow}. \tag{15}$$

The parameter $repow$ is the power which increases the fracture energy with strain rate and $f'$ is internally calculated by the program and it describes the yield strength before application of rate effect. The more detailed description of the model is presented in user's manual for Ls-Dyna concrete material model 159 [14, 16].

The set of all constitutive parameters is presented in Table 1. The parameters for concrete B30 are described based on numerical and experimental tests [14–21]. The results for uniaxial tension and compression for different strain rates are presented in Fig. 5. The strain rate hardening of the material is presented. The softening appears after initiation of damage and is strain rate sensitive.

These numerical tests are in agreement with real behaviour described by Figs. 2-C and 2-D. According to the CEB recommendations that follow the experimental results the dynamic strength of concrete increases together with strain rates. The existing failure criterion which depends on state of stress and strain rates is obvious. Failure of concrete is connected with the accumulation of energy (mainly the elastic energy) in time. In this case it is possible to describe the time up to failure according to cumulative failure criterion. The first time this kind of failure criterion was proposed by Campbell in 1953 [22]. The generalization of cumulative failure criteria [3, 22] used to simulate the dynamic behaviour of concrete in Spall Pressure Hopkinson Bar SPHB tests [3, 23]. The compressive dynamic behaviour of the material is tested using Split Hopkinson Pressure Bar (SHPB) [24, 25].

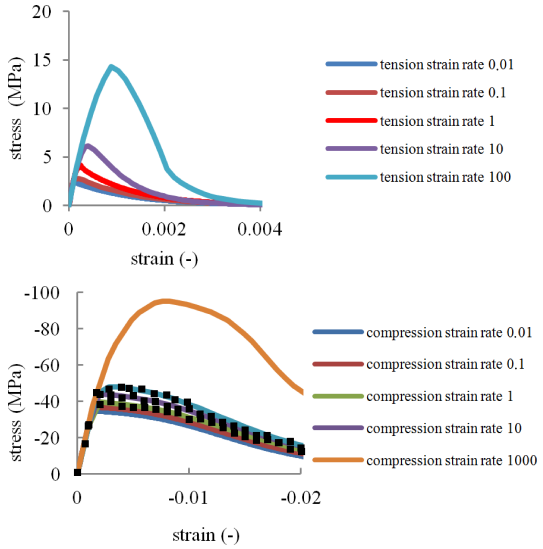


Fig. 5. The strain rate sensitivity for concrete class B30 for tension and compression

## 4. Numerical results

Many numerical tests were performed. Selected results are presented below for the case of one concrete slab and at the end of this section for the case of concrete slabs set. The results for reinforced (1, 2 or 3 layers) single concrete slab are also presented.

Firstly, the single pure concrete slab is considered. The analyses show the influence of mesh density in FEM and particle distance in SPH. The results of numerical simulations are presented in Fig. 6. The two discretisations are shown with 2 mm and 1 mm. The results prove that the blast loading could estimate properly the structural behaviour for both FEM and SPH. The maximum pressure and reactions (sum of the all node forces on perimeter) is independent of the discretisation density (Fig. 6-B – FEM and Fig. 6-D – SPH) for all considered mass charges. The pressure and reaction peaks appear in the same time for coarse and fine discretisation (Fig. 6-A – FEM and Fig. 6-C – SPH).

The maximum of the reaction forces due to explosion of charge are similar for two considered numerical methods, see Table 2. The quantitative difference for fine discretisations is about 15% (34.6 MN – FEM and 39.3 MN – SPH). The maximum pressure and the reaction appear at the beginning of the failure process (from 350 $\mu$s to 700 $\mu$s dependently on the mass of charge).

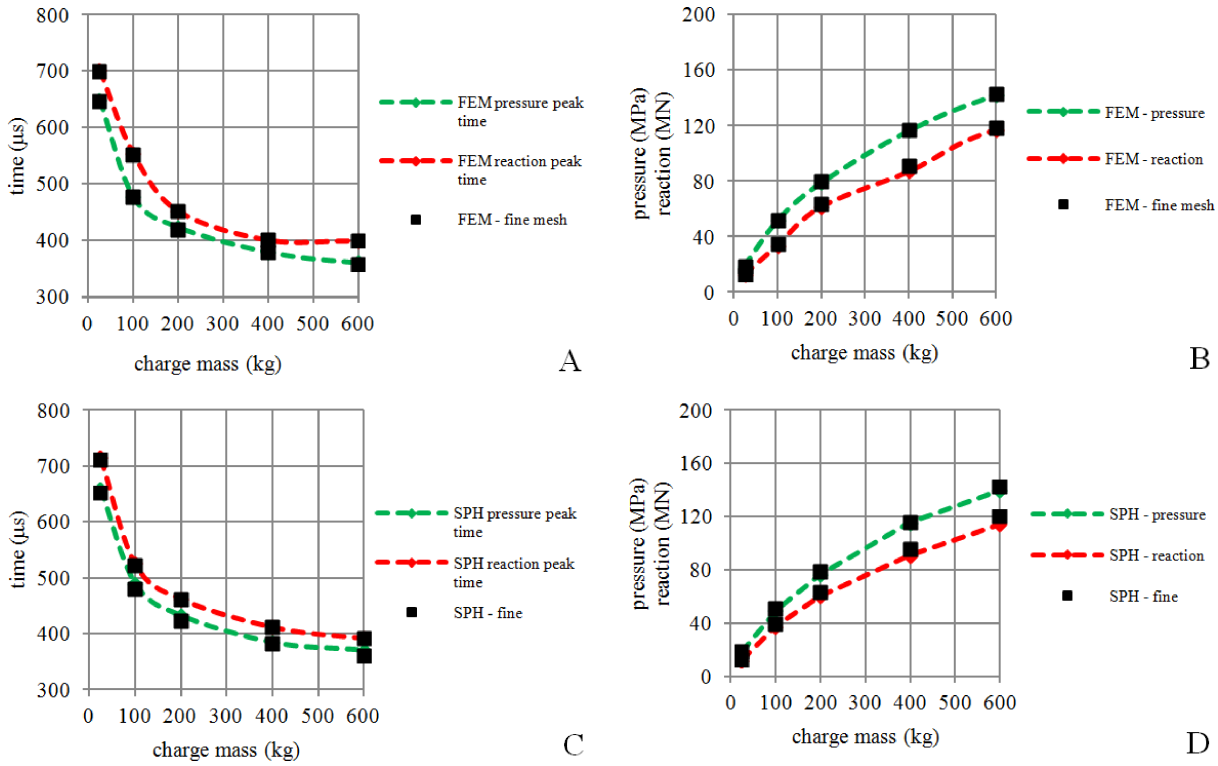


Fig. 6. Comparison of the maximum pressures, reactions and times of its appearance for FEM (A,B) and SPH (C,D)

Table 2

The values of maximum pressure and maximum reaction forces together with the time of its appearance for two considered numerical methods

| Mass charge [kg] | Results | FEM -fine | SPH - fine |
|---|---|---|---|
| 100 kg | max pressure | 51.5 MPa | 51.2 MPa |
| | at time | 476 $\mu$s | 479 $\mu$s |
| | max reaction force | 34.6 MN | 39.3 MN |
| | at time | 552 $\mu$s | 521 $\mu$s |

The previous results give the global information about the loading and dynamic response of concrete slabs. The local analysis was also performed for all considered cases. Below, the failure pattern of the single concrete slab loaded by explosion of 100 kg of TNT is presented in two time instants, Fig. 7. In the case of SPH method, the circular spall is clearly visible together with the distribution of damage parameter and velocities, see Fig. 8. The maximal velocity of the nodes in FEM and in SPH are very close and equal to 20 m/s but in FEM simulation the elements disappear during explosion loading. The problem of mass disappearing has a big influence if the parts of the first concrete slab impact onto the second one. Using the SPH method of the spall particles (Fig. 8) may impact onto the second slab of the set.

In numerical simulations, the problem appears if two concrete slabs placed a certain distance apart which is considered, see Fig. 1. After an explosion the first slab is damaged but later the pieces impact the second one and the finite elements disappear after the failure criterion in concrete is met. The impact velocity is close to 33 m/s for mass of charge 200 kg of TNT, see Fig. 9. Most of the finite elements are deleted in this case, see Fig. 9. The same problem does not exist when using SPH method. It will be presented later in this chapter.

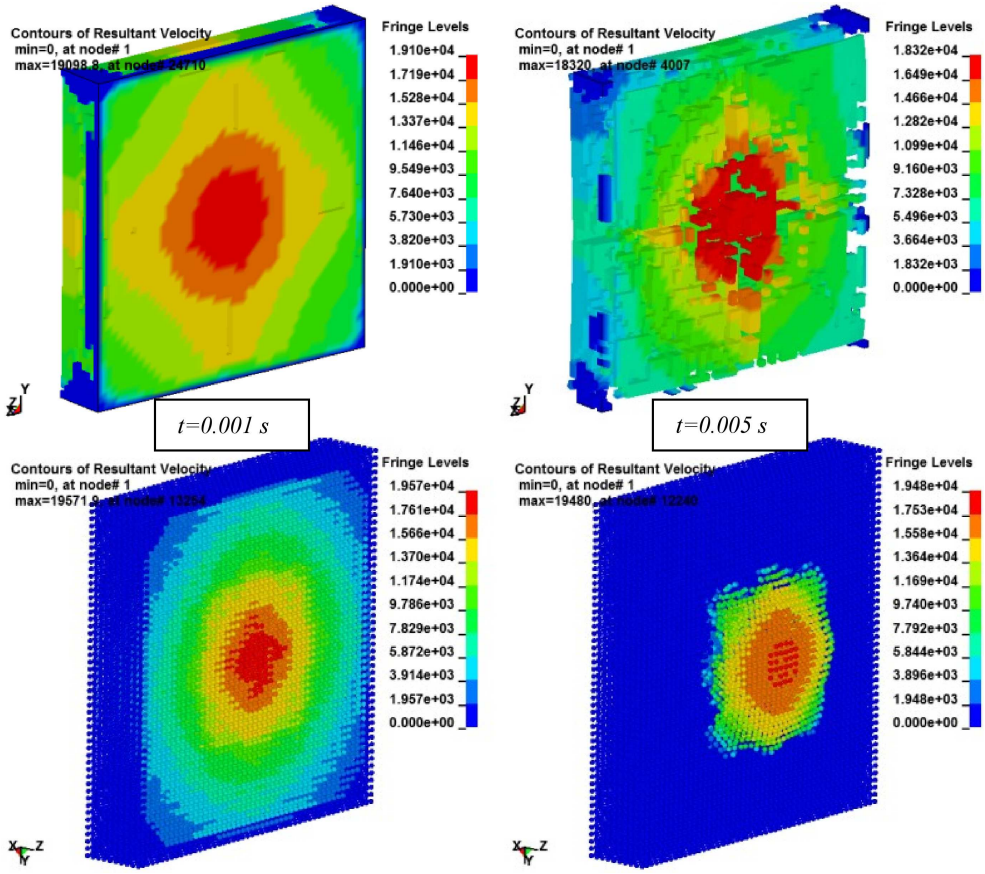


Fig. 7. The comparison of the velocities after explosion of 100 kg of TNT for two considered methods: FEM (top) and SPH (bottom)

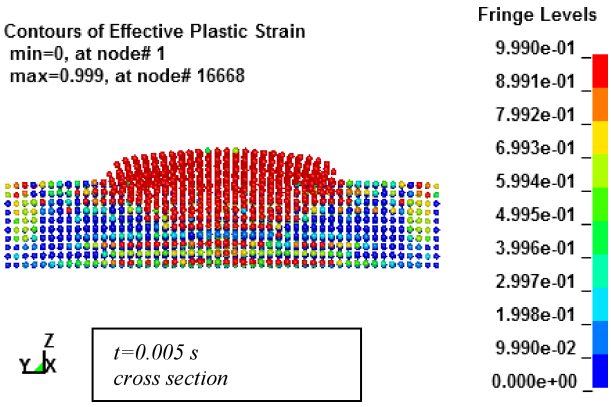


Fig. 8. The spall in concrete slab modelled by SPH due to explosion of 100 kg of TNT

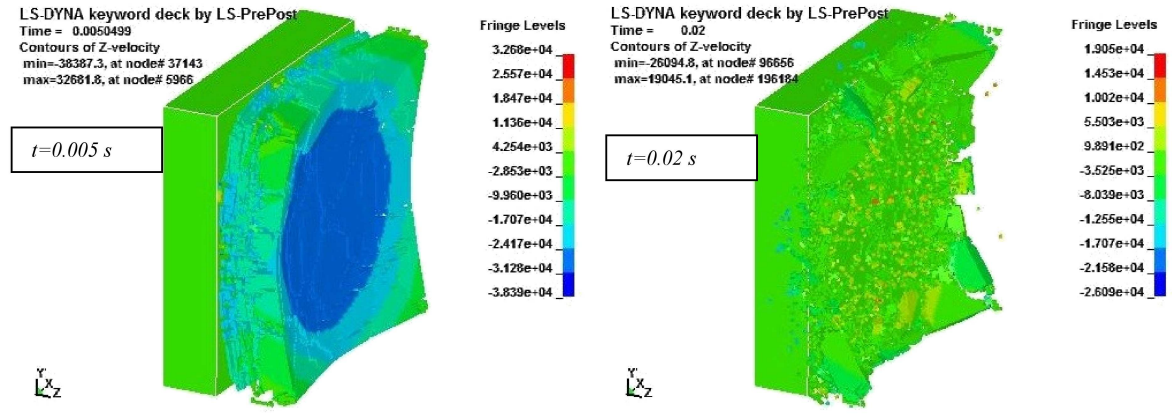


Fig. 9. Annihilation of the finite elements during explosion impact of 200 kg of TNT – independently of the mesh size

The next analyses use the SPH method. The examples consider a single slab and the set of two slabs. The results for only one mass of charge equal 200 kg of TNT are presented. The other simulations for all considered masses of charge and for fine SPH particles distance were also considered. We can conclude that the particle distance in SPH or finite element size in FEM have not a crucial influence on quality and quantity of numerical results in both methods after taken into account the information which are discussed in Appendix A.

In Fig. 10 the field of velocity is presented for a single plate and mass of charge 200 kg. The maximal velocity of spall which appears in this case is about 33 m/s. In case of single plate this large part of the pure concrete structure flies (after spalling) – move with this high velocity. It may impact onto the second obstacle (slab) which may save the structure interior and people behind this obstacle.

We consider also the case with two parallel concrete slabs with the gap of 10 cm between them, see Fig. 1. Using the second slab has a positive influence on the velocity of the spall in the first one which is created after explosion. The spall impacts onto the second slab with the velocity 33 m/s. The maximal velocity of the second slab is 13 m/s but it does not collapse the second plate due to energy dissipation. The total kinetic energy of the system is close to zero at the end of the process. In Fig. 11 we see failure pattern of the first slab and only a few parts of the second one are damaged. For larger mass of charge the situation is different and the system collapses due to explosion connected with impact.

The cases of reinforced single slabs are also discussed and the results are presented in Fig. 12. We assumed 34GS steel bars with diameter 4 mm (space 100 mm). The reinforcement is build with 1, 2 or 3 layers. The authors have assumed that the SPH particle are also the nodes of beam elements. The reinforcement (beam elements) is embedded into SPH particles.

In Fig. 12-A the displacement of reinforced slab (1 layer) is presented for three charges 25, 50 and 100 kg. The reinforcement decrease the slabs failure and the maximal displacements are respectively about 75 mm, 127 mm and 220 mm. When using reinforcement also the velocity decrease after reaching the maximal value of 13 m/s, 26.2 m/s and 44.7 m/s. The important results of presented simulations are also that the use of additional layers of reinforcement dose not influence the maximal velocities too much. For two layers the maximal velocities are respectively 12 m/s, 24 m/s and 41 m/s. After adding the third layer of reinforcement in the middle of slab the maximal velocities are 11 m/s, 22 m/s and 41 m/s. The reinforcement carries the huge part of the explosion power and concrete is damaged only locally (opposite side).

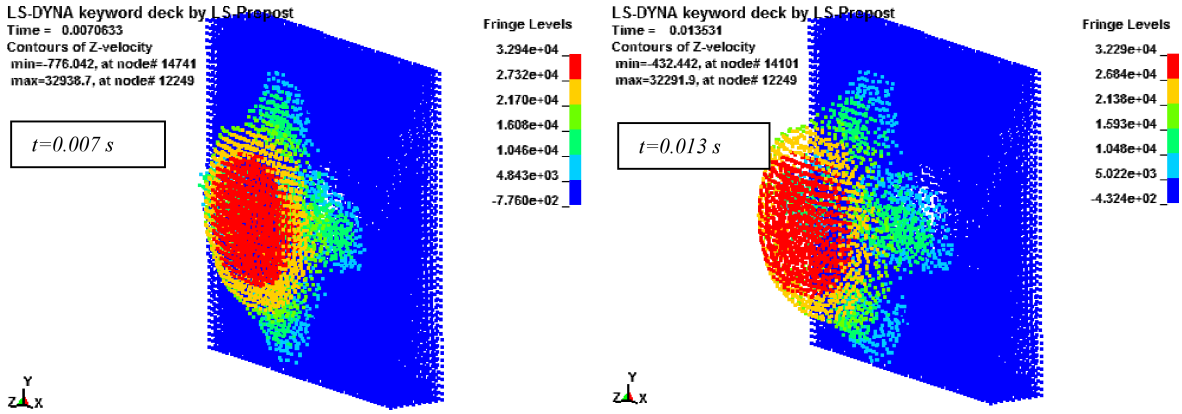


Fig. 10. Velocity field for single plate SPH model and mass of charge 200 kg for two time instances

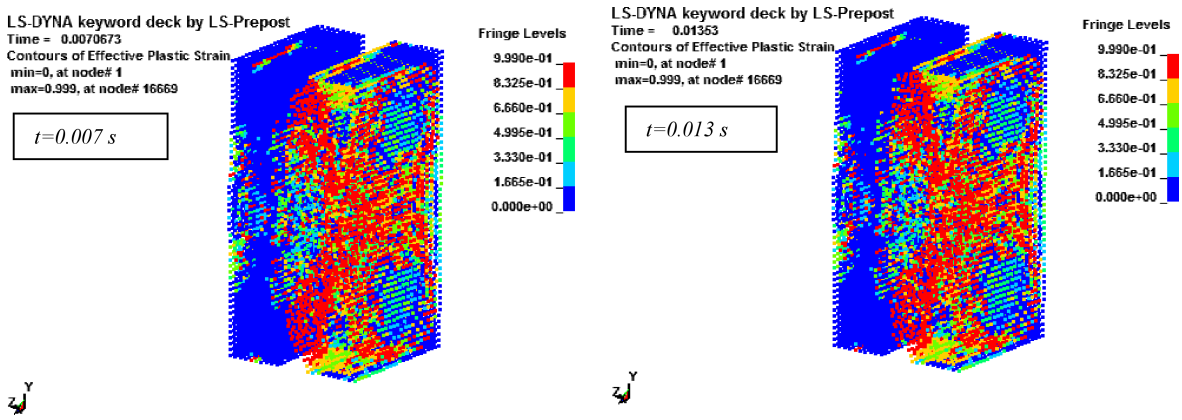


Fig. 11. Damage field for case of two concrete slab and mass of charge 200 kg

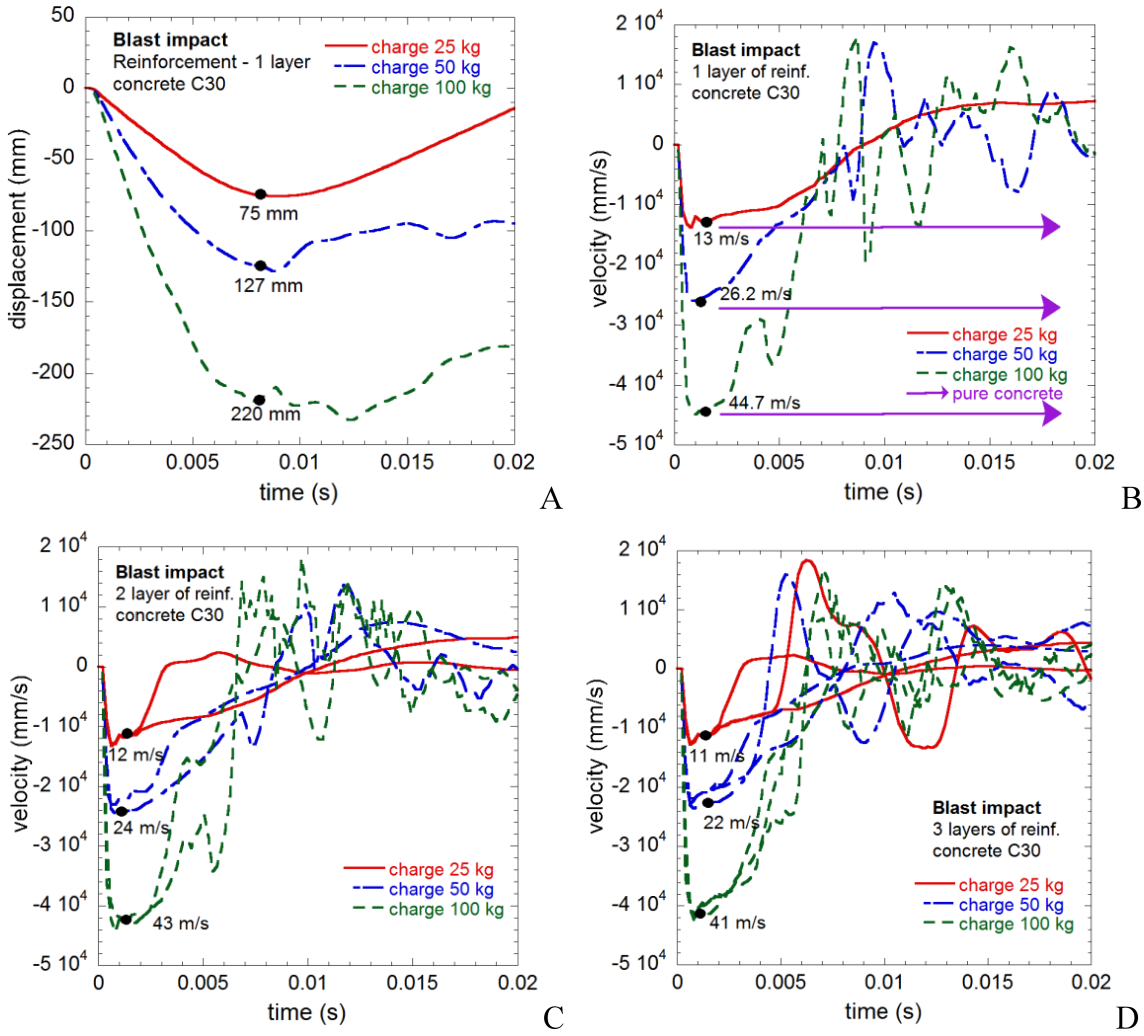


Fig. 12. A – Displacement of reinforcement slab (1 layer) for three charges; B – Velocity of reinforcement slab (1 layer) for three charges; C – Velocity of reinforcement slab (2 layer) for three charges; D – Velocity of reinforcement slab (3 layer) for three charges

## 5. Final conclusions

In the paper the efficiency and usefulness of two methods, often used in numerical simulations, are compared. The mechanisms of failure of the single concrete slab and a set of two concrete slabs are discussed. The influence of the mass of charge is also presented. The influence of reinforcement layers is discussed as well.

The several crucial conclusions can be drown below:

- The dependency for simulation of slab failure due to explosion was checked. Using the regularised material model

from ls-dyna library, the problem of mesh dependency on numerical results is under control.

- Both methods predict very similar times of appearance of the maximum pressure and maximum reactions independent of the finite element size and the particles distance.
- Failure patterns are more adequate and real using the SPH method. Using the FE method a lot of mass is deleted particularly for bigger charges that create the non- physical problems.
- Analysing the dynamic behaviour of the system of concrete slabs – we can conclude that SPH is better suited, especially if the parts of the one blasted slab impact onto the second one.
- Analysing the influence of the reinforcement – we can conclude that adding the second or the third layer of reinforcement does not influence very strongly the deformation and maximal velocity of the concrete slabs.

Future work will consider other safety applications like slabs with the different dimensions and shapes, other reinforcement and configurations - composite of the steel, concrete and other composites. Future work can describe also residual strength of the civil engineering structures [25].

In Appendix the influence of SPH parameters like: loading velocity effect, particles distance effect, smoothing length effect and computation time effect are presented. The proper understanding of these parameters has an important influence on the results of simulations.

## Appendix – SPH method

This part of the paper considers the parameters of the SPH method and also compares some results obtained by SPH and FEM methods. The SPH method is one of the possibility in the whole group of meshless methods. It is particle collocative method which was developed firstly by Lucy, Gingold and Monaghan [11, 12, 26]. SPH uses Lagrangian formulation of deformation together with dynamic explicit method of time integration, which is conditionally stable. It solves the conservation of mass, momentum and energy partial differential equations [27]. The SPH method was firstly developed to solve astrophysics problems and later was used to avoid the problems with extreme mesh deformations in FEM for impact and penetrations problems in Solids. The accuracy is not high compared to FE (instability in tension, consistency). The difference is the absence of the grid. The governing equations are solved based on particles computational framework.

In comparison of the SPH method with FE method the simulation of simple compression (uniaxial) is used. The material model used in the following simulations has been presented before in Subsec. 2.1 together with constitutive parameters.

**Loading velocity effect.** For the analysis of the loading velocity only one SPH model is used (SPH-10), Fig. A-1. It means that volume 10x10x10 cm is discretized with $10\times10\times10$ grid. Total number of particles in this case is equal 1000. The vibrations are visible clearly for loading velocity 1000 mm/s. The differences in stiffness and material strength are observed. Next simulations use loading velocity 100 mm/s. It responds to strain rates equal to 1 1/s. The stiffness and the strength of considered material in SPH-10 (red line) is far from FE model results (black line), see Fig. A-2 (15% difference). In the next sections the solution variables change to better agreement of SPH and FE methods.

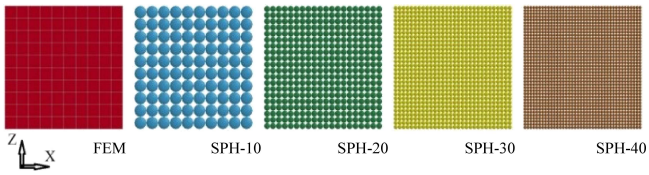


Fig. A-1. FE and SPH models with different particles density

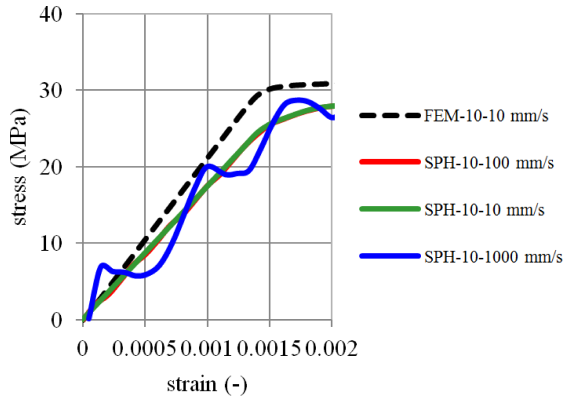


Fig. A-2. Loading velocity effect

**Particles distance effect.** In Fig. A-3 there is a presentation of the main parameters which describe the solution using SPH. In this section parameter d (particles distance) is considered. It is an important variable if we want to obtain the results which are closer to FEM. If the distance between particles decreases the solution using SPH is closer to the FE solution, see Fig. A-4. The results for SPH-30 and SPH-40 are almost identical and the solution is very close to FE (5% difference). In the next Section we consider the next important SPH parameter the so called smoothing length h to check the conditions which drives to the better solution.

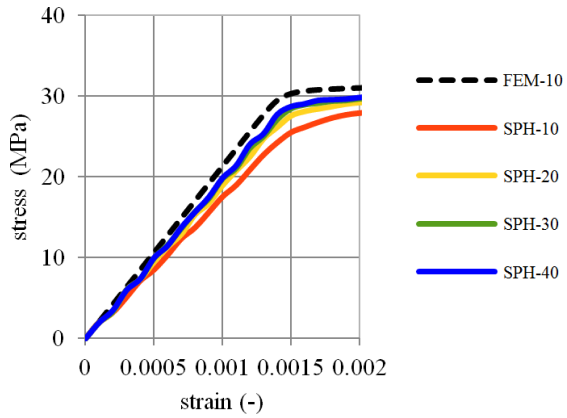


Fig. A-3. Particle distance effect

**Smoothing length effect.** The smoothing length meaning is presented in Fig. A-4. In this section it is presented how the smoothing length effects the simulations results. Figure A-5 shows that for smoothing length (1.05) the SPH results coincide with FE (1% of difference). It means that this parameter is very important in this kind of numerical analyses. In this case the results are converged and this value of parameters may be used in the next simulation. The last one variable is the computation time effect. It is presented in the next section.

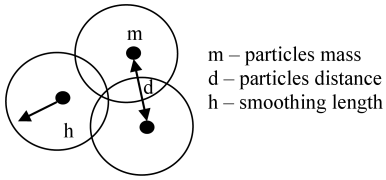


Fig. A-4. The main parameters using SPH

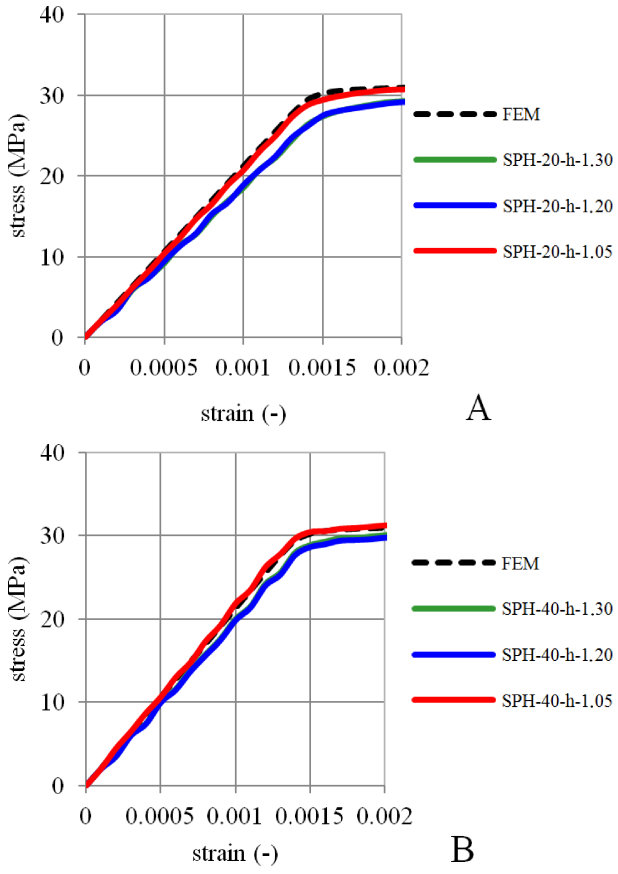


Fig. A-5. The comparison of SPH and FE method results for two particles distance SPH-20 and SPH-40 and different smoothing element lengths 1.2 (default), 1.3 and 1.05

**Computation time effect.** The computation time increases with decreasing the loading velocity. Generally, for using SPH the computation time is higher than for FEM. The correlation with the number of particles is nonlinear in SPH, see Fig. A-6.

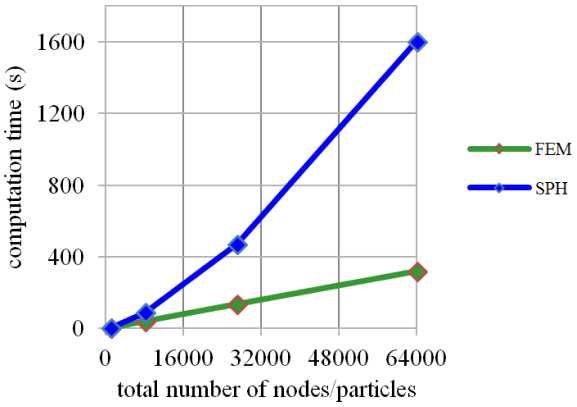


Fig. A-6. Computation time effect

**Acknowledgements.** The authors thank the Ministry of Science and Higher Education for financial support under the project: R00 0097 12 "Security of critical infrastructure through passive system of protection".

REFERENCES

[1] R. Radvanovsky and A. McDougall, *Critical Infrastructure: Homeland Security and Emergency Preparedness*, ed. 2, Taylor and Francis, New York, 2010.
[2] J. Sullivant, *Strategies for Protecting National Critical Infrastructure Assets*, John Wiley and Sons, New Jersey, 2007.
[3] T. Krauthammer, *Modern Protective Structures*, Taylor and Francis, New York, 2008.
[4] R. Horonjeff, F.X. McKelvey, W.J. Sproule, and S.B. Young, *Planning and Design of Airports*, ed. 5, Mc Graw Hill, New York, 1994.
[5] P.S. Bulson, *Explosive Loading of Engineering Structures*, Taylor and Francis, New York, 1997.
[6] D. Cormie and G. Mays, *Blast Effects on Buildings*, ed. 2, Thomas Telford, London, 2009.
[7] M.Y.H. Bangash and T. Bangash, *Explosion-Resistant Buildings*, Springer, Berlin, 2006.
[8] Ch.L. Mader, *Numerical Modelling of Explosives and Propellants*, ed. 3, Taylor and Francis, New York, 2008.
[9] P. Sielicki and T. Łodygowski, "Pressure loadings on structure after explosion", $7^{th}$ *ISIE* 1, CD-ROM (2010).
[10] O. Zienkiewicz and R. Taylor, *The Finite Element Method*, ed. 6, Elsevier Butterworth, London, 2005.
[11] R.A. Gingold and J.J. Monaghan, "Smoothed particle hydrodynamics, theory and application to non-spherical stars", *Monthly Notices of the Royal Astronomical Society* 181, 375–389 (1977).
[12] L.B. Lucy, "A numerical approach to testing of the fusion process", *Astronomical J.* 88, 1013–1024 (1977).
[13] G. Randers-Pehrson and K.A. Bannister, *Airblast Loading Model for DYNA2D and DYNA3D, ARL-TR-1310*, Army Research Laboratory, New York, 1997.
[14] *Users Manual for Ls-Dyna Concrete Material Model 159*, FHWA-HRT-05-062, U.S., Department of Transportation, 2007.
[15] T. Jankowiak and T. Łodygowski, "Quasi-static failure criteria for concrete", *Archives of Civil Eng.* LVI 2, 123–154 (2010).
[16] *LS-Dyna Theory Manual*, compiled by John O. Hallquist, 2010.

[17] P. Bischoff and S. Perry, "Compressive behaviour of concrete at high strain rate", *Materials and Structures* 24, 425–450 (1991).

[18] A. Brara and J.R. Klepaczko," Experimental characterization of concrete in dynamic tension", *Mechanics of Materials* 38, 253–267 (2006).

[19] H. Kupfer, H. Hilsdo, and H. Rusch, "Behavior of concrete under biaxial stresses", *ACI J.* 66, 656–666 (1969).

[20] A.M. Neville, *Properties of Concrete*, John Wiley and Sons, New Jersey, 1996.

[21] S. Swanson and S. Green, *Static Constitutive Relations for Concrete,* Kirtland Air Force Base, U.S. Air Force Weapon Laboratory, Kirtland, 1973.

[22] T. Jankowiak, *Quasi-static and Dynamic Failure Criteria of Concrete*, Publishing House of Poznan University of Technology, Poznan, 2011, (in Polish).

[23] T. Jankowiak, J.R. Klepaczko, and T. Łodygowski, "Numerical modeling of wave propagation and interaction in bars", *Foundations of Civil and Environmental Eng.* 7, 187–199 (2006).

[24] T. Jankowiak, A. Rusinek, and T. Łodygowski, "Validation of the Klepaczko–Malinowski model for friction correction and recommendations on split Hopkinson pressure bar", *Finite Elements in Analysis and Design* 47, 1191–1208 (2011).

[25] X. Bao and B. Li, "Residual strength of blast damaged reinforced concrete columns", *Int. J. Impact Eng.* 37, 295–308 (2010).

[26] J.J. Monaghan, "An introduction to SPH", *Computer Physics Communications* 48, 88–96 (1988).

[27] R.J. LeVeque, *Numerical Methods for Conservation Laws*, ed. 2, Birkhauser Verlag, Berlin, 2006.